MEASUREMENTS OF SAND TRANSPORT AND ITS UNDERLYING PROCESSES UNDER LARGE-SCALE BREAKING WAVES (SANDT-PRO)

Jan S. Ribberink (1), Dominic A. van der A (2), Joep van der Zanden (3),
Tom O'Donoghue (4), David Hurther (5), Iván Cáceres (6) & Peter D. Thorne (7)

(1) University of Twente, the Netherlands, E-mail : j.s.ribberink@utwente.nl
(2) University of Aberdeen, UK, E-mail : d.a.vandera@abdn.ac.uk
(3) University of Twente, the Netherlands, E-mail : j.vanderzanden@utwente.nl
(4) University of Aberdeen, UK, E-mail : t.odonoghue@abdn.ac.uk
(5) LEGI-CNRS, France, E-mail : david.hurther@hmg.inpg.fr
(6) Universitad Politècnica de Catalunya, Spain, E-mail: i.caceres@upc.edu
(7) National Oceanographic Centre Liverpool, UK, E-mail : pdt@noc.ac.uk

In this paper, we present the first results of a measurement campaign done in the Barcelona CIEM wave flume from October 2013 to January 2014. The aim of the experiments was to improve our understanding of sediment transport processes in the near-shore region. In particular, we focused on the effects of (1) wave breaking and (2) wave irregularity on net sediment transport rates and sediment transport processes. High-resolution measurements were obtained using advanced instrumentation, deployed from a custom-built measuring frame that was both horizontally and vertically mobile. These instruments provide detailed insights in the vertical distributions of sediment fluxes. Preliminary results from the breaking-wave experiments show an onshore transport of sediment prior to breaking, likely to be dominated by wave-nonlinearity effects, and an offshore sediment flux shoreward of breaking, where the sediment fluxes are undertow-dominated.

1. INTRODUCTION

The complex interactions between hydrodynamics and sediment transport processes in the near-shore region are not yet understood at a level of detail required for accurate model predictions. This holds in particular for the effects of wave irregularity and wave breaking, and is primarily caused by a lack of detailed experimental hydrodynamic and sediment flux data. Previous breaking-wave experiments had their focus on hydrodynamics and turbulence distributions (e.g. Boers, 2005), in some cases in combination with bed morphology and suspended sediment transport (Roelvink and Reniers, 1995; Maddux *et al.*, 2006), while detailed measurements under irregular waves are somewhat limited, especially at large scale (O'Hara Murray *et al.*, 2012). Our research aim is to uncover further the physical processes that drive sand transport under different types of regular breaking and irregular non-breaking waves. This is achieved through a new series of mobile-bed wave flume experiments using advanced measuring instruments within the EU Hydralab IV project SandT-Pro. Compared to earlier experiments, the new experiments yield greater detail and insights into the bottom boundary layer processes and near-bed sediment transport fluxes.

Two types of experiment were conducted, each with its own research aims: (i) Experiments involving regular breaking (RB) waves, focusing on the effects of wave breaking on near-bed sediment dynamics, including the influence of additional stirring caused by breaking on the (especially near-bed) sediment fluxes, and the effects of horizontal advection processes of turbulence and suspended sediment; (ii) Experiments with irregular non-breaking (INB) waves, focusing on turbulence and sediment pumping under wave groups, the effect of wave sequence on the wave-related sediment flux in the suspension layer and the comparison of net transport rates for "equivalent" regular and irregular wave conditions.

2. DESCRIPTION OF EXPERIMENTS

2.1 BED SET-UP AND WAVE CONDITIONS

The experiments were done at the CIEM flume of UPC, Barcelona, from October 2013 to January 2014. The initial bed consists of an offshore linear slope (1:10 during most experiments), followed by a long horizontal test section (1.35 m height) and a fixed parabolic beach (Figure 1). The bed material consists of medium-grained sand with a D_{50} of 0.25 mm.

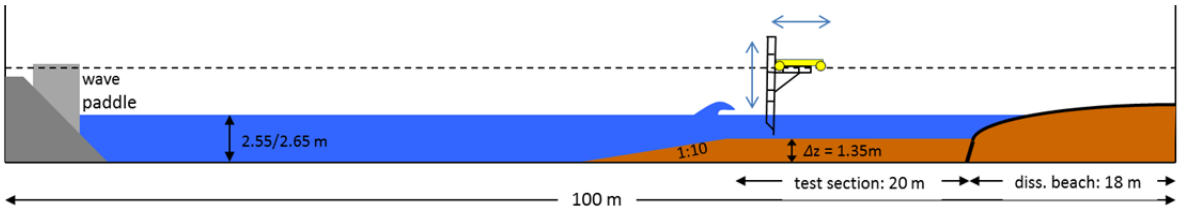

Figure 1: Experimental set-up.

An overview of both the RB and the INB wave conditions is given in Table 1. In general, wave conditions were selected to have high near-bed orbital velocities. The RB wave conditions were designed such that waves would break at the beginning of the horizontal test section. For these experiments, the high near-bed velocities induced bedload transport in the sheet-flow regime in the zone before breaking. Regular waves were used in order to obtain good convergence of measured intra-wave sediment transport processes through ensemble-averaging. The characteristics of the breaking wave were varied by using various wave heights and water depths at the wave paddle (d_0) and by changing the initial slope, resulting in the two conditions RB1 and RB2.

Table 1: Overview wave conditions. d_0 is the water depth at the wave paddle; T is the period of the short wave; H is the wave height with subscripts *rms*, *s* and *max* representing the root-mean-squared, significant, and maximum wave height of the wave group respectively; T_g is the period of the group; and n is the number of short waves per group.

Regular Breaking (RB)								
Run	***d0* (m)**	**Slope**	***T* (s)**	***H* (m)**	**# runs**	**Duration runs (min)**		**Remarks**
RB1	2.55	1:10	4.0	0.85	22	15 to 20		Plunging
RB2	2.65	1:20	4.0	0.95	26	20 to 30		Weakly plunging
Irregular Non-Breaking (INB), grouped waves								
Run	***d0* (m)**	**Slope**	***T* (s)**	***H*$_{rms}$ (m)**	**H$_s$ (m)**	***H*$_{max}$ (m)**	***T*$_g$ (s)**	***n***	**Remarks**
IGB1	2.65	1:10	4.4	0.49	0.69	0.69	41.8	10	Bichromatic, fully modulated
IGB2	2.65	1:10	4.4	0.49	0.69	0.69	28.6	7	Bichromatic, fully modulated
IGB3	2.65	1:10	4.4	0.49	0.69	0.62	41.8	10	Bichromatic, partially modulated
IGM1	2.65	1:10	4.4	0.49	0.69	0.79	44.0	10	Waxing, fully modulated
IGM2	2.65	1:10	4.4	0.49	0.69	0.79	44.0	10	Waning, fully modulated
Irregular Non-Breaking (INB), monochromatic reference cases								
Run	***d0* (m)**	**Slope**	***T* (s)**	***H* (m)**	**# runs**	**Duration runs (min)**		**Remarks**
IM1	2.65	1:20	4.4	0.49	3	22		H equal to H_{rms} of groups
IM2	2.65	1:20	4.4	0.69	3	22		H equal to H_s of groups
IM3	2.65	1:20	4.4	0.79	2	22		H equal to H_{max} of IGM groups

For the INB experiments, two type of non-breaking wave conditions were realized: regular (monochromatic) waves and bichromatic wave groups. The wave groups were generated by modulating a regular (short) wave time-series as follows:

$$\eta(t) = A(t)a\sin\left(\frac{2\pi}{T}t\right) \tag{1.1}$$

in which a is the amplitude of the short wave, T is the short wave period (T = 4.4 s) and $A(t)$ is the modulating wave envelope. In its simplest form $A(t)$ consists of a sine wave modulation as follows:

$$A(t) = 1 + M\sin\left(\frac{2\pi}{T_g}t\right) \tag{1.2}$$

where M is the amplitude modulation coefficient (M = 0 is no modulation, M = 1 is full modulation, resulting in $H = 4a$), T_g is the period of the wave group ($T_g = nT$ with n the number of short waves in a group). Conditions IGB1 and IGB2 are based on Eq. (1.1) and (1.2) with M = 0.9, the only difference being the number of waves in the group n = 7 (IGB1) and n = 10 (IGB2). For the other two group conditions (IGM1 and IGM2) a smooth sawtooth shaped modulation function is used based on the Generalised Sawtooth (GSAW) function of Malarkey and Davies (2012):

$$A(t) = 1 + M\arctan\left(\frac{b\sin\left(\frac{2\pi}{T_g}t\right)}{1 - b\cos\left(\frac{2\pi}{T_g}t\right)}\right)\arctan\left(b\left(1-b^2\right)^{-1/2}\right)^{-1} \tag{1.3}$$

Here, $b = 2\beta - 1$ and β is a factor that describes the degree of forward- or backward-leaning ("sawtoothiness"), i.e. $\beta > 0.5$ leads to a forward-leaning sawtooth shape, $\beta < 0.5$ leads to a backward-leaning sawtooth shape and $\beta = 0.5$ is a purely sinusoidal function, similar to Eq. (1.2). The target 'waxing' and 'waning' wave groups IGM1 and IGM2, based on Eq. (1.3), are shown in Figure 2.

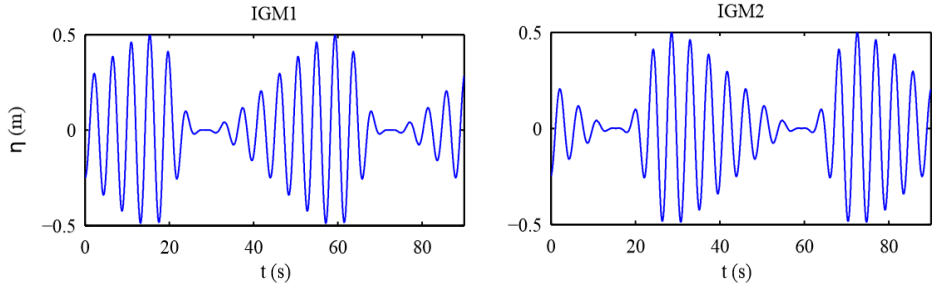

Figure 2: Target wave groups conditions IGM1 (waxing, left) and IGM2 (waning, right).

2.2 INSTRUMENTATION AND PROCEDURES

Detailed process measurements were obtained using a vertical array of state-of-the-art instrumentation, deployed from a mobile measuring frame that was custom-built at the University of Twente. This frame consists of a steel construction of slim rods, mounted to the bottom of a horizontally-mobile carriage located above the flume (Figure 1). The frame can be vertically repositioned with O(mm) accuracy using a spindle. The frame was designed such that it was as stiff as possible, while at the same time flow perturbations were tried to be minimized.

A range of various measuring instruments for sediment concentrations and flow velocities was mounted to the mobile frame instruments (Figure 3). Water velocities (two components) were sampled simultaneously using a High-Resolution Acoustic Concentration and Velocity Profiler (HR-ACVP). This prototype system is currently developed within the project Hydralab IV-WISE on the basis of the

ACVP technology described in Hurther *et al.* (2011). In addition, a Nortek Vectrino Profiler was used to measure near-bed velocities and turbulence in three components. Near-bed sediment concentrations were measured using the HR-ACVP (vertical profile) and an Optical Backscatter Sensor (OBS; point measurement near the bed). Higher in the vertical, velocity and concentration profiles were measured using ADVs, OBSs and an AQUAscat Acoustic Backscatter Sensor (ABS). The concentration measurements are calibrated and verified with suction measurements of suspended sediment, obtained with a 7-nozzle Transverse Suction System (TSS). The suction samples were sieved and dry-weighted to yield time-averaged concentrations and, later, sampled for laser-diffraction-based grain-size analysis.

Moreover, two CCM+ (Conductivity Concentration Measurement) tanks (Van der Zanden *et al.*, 2013) for sheet flow sediment concentration and particle velocity measurements were installed in the sand bed, below two additional HR-ACVP systems. The latter were mounted to two separate fixed wall frames above the CCM+ tanks. Water surface elevation was measured along the flume with 13 resistive wave gauges and, near the breaker location, with 9 pore pressure transducers at 1 m intervals. Total net transport rates are obtained from mass conservation using pre- and post-test bed profiles measured with acoustic bed profilers.

During the RB experiments, process measurements were obtained at various cross-shore positions while the bed profile evolved in order to measure the various sand transport processes driven by the breaking waves. For the INB cases, measurements were concentrated at one cross-shore position in the middle of the horizontal test section as flow above the test section was assumed uniform.

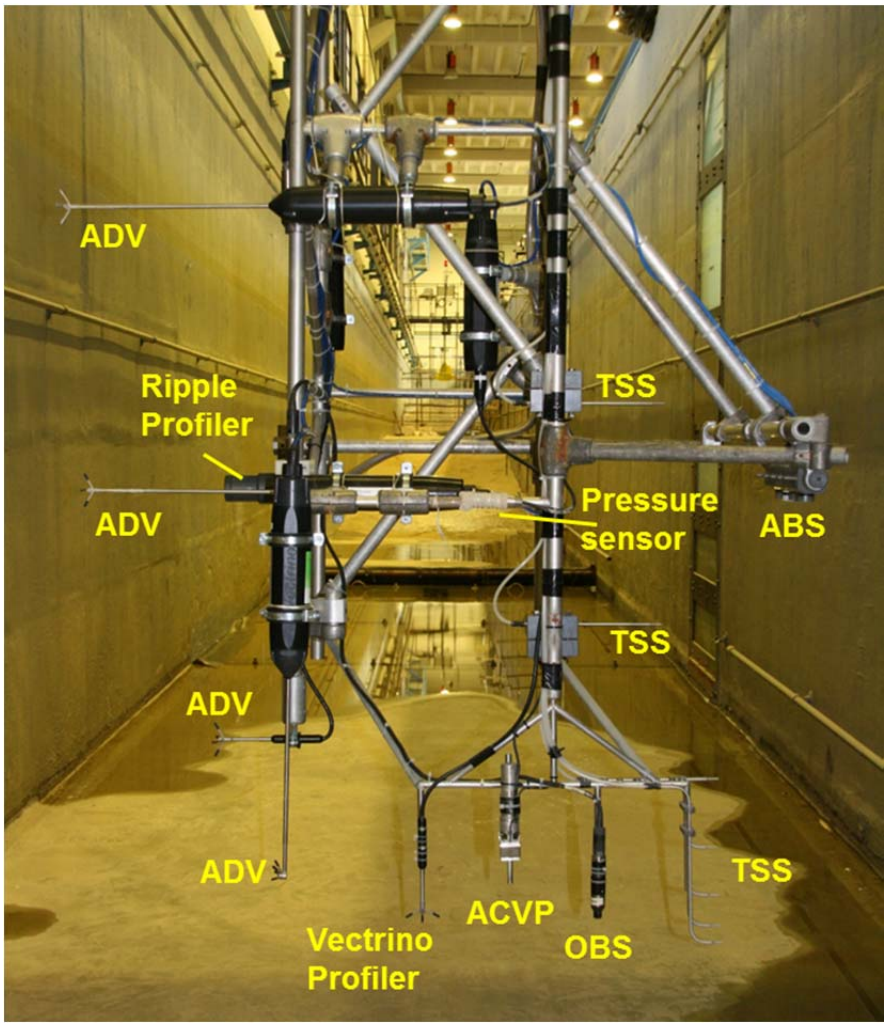

Figure 3: Instrumental set-up on the mobile frame.

3. RESULTS AND DISCUSSION (BREAKING WAVES)

In the present paper, preliminary results of the measured sand transport rates and processes for condition RB1 (regular breaking waves) are presented and discussed. We will first present the morphologic evolution of the bed and the net sediment transport rates, and will later show a few detailed measurements that help explain the morphodynamics.

3.1 MORPHOLOGIC EVOLUTION AND SAND TRANSPORT

The evolution of the bed profile is shown in Figure 4 (upper graph). From left to right we can distinguish in the initial profile (red line) the 1:10 bottom slope (x=34 to 47 m), followed by the horizontal test section, and finally the beginning of the fixed parabolic beach (indicated by the bump at x=68.5 m). The plot includes the position of the breaking point, defined here as the cross-shore location with the largest reduction in wave heights.

After the start of the experiment, the continuous breaking of the regular waves promoted the growth of a breaker bar and trough. After approximately 4.5 hours of wave action, the breaker bar and trough are clearly visible in the measured profile (black line). Further observations reveal large bedforms at the inclined part of the profile (x<50 m), followed by a flat bed in the shoaling zone until the breaking point (x=50 to 56 m). The latter suggests that bedload transport is in the sheet-flow regime here. Moving from the breaking point towards the surf zone a gradual transformation of a flat bed (x=56 to 58 m) to large quasi-2D crescentic bedforms (x=58 to 61 m) can be seen, followed by 3D ripples in the surf zone (x=61 to 68 m).

Net time-averaged sediment transport rates for the 275 minutes were obtained by applying a mass-conservation method as described for instance by Baldock *et al.* (2010). Results, shown in Figure 4 (bottom graph), reveal an onshore (positive) sediment flux before breaking and an offshore (negative) flux shoreward of breaking, which together contribute to building the breaker bar. Around the breaking point, the transport gradient is large which underlines the importance of breaking-induced sediment transport processes for morphologic evolution in the near-shore region.

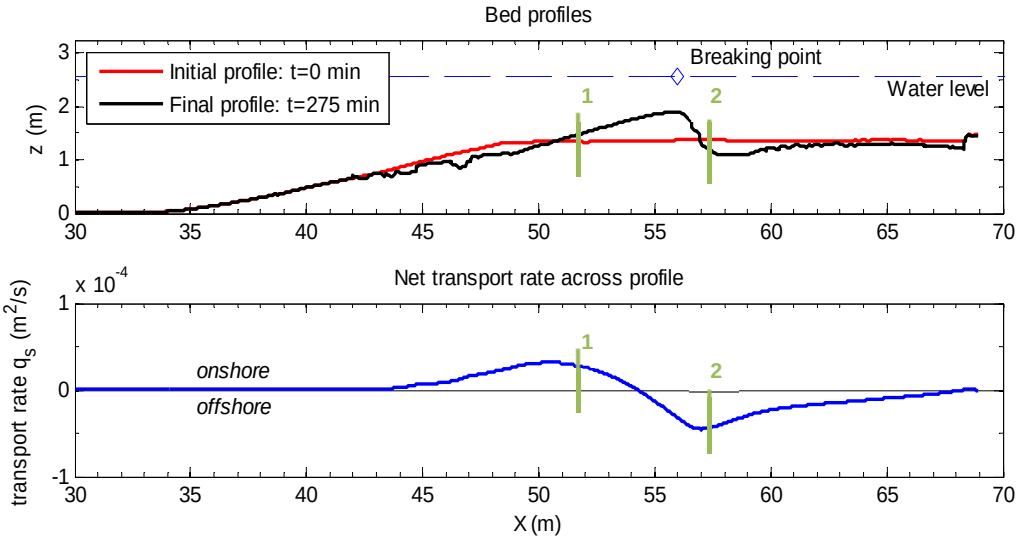

Figure 4: Profile development (upper) and net transport rates (lower) for RB1 experiment (after 275 minutes). Green vertical bars indicate positions of fixed frames.

3.2 NEAR-BED VELOCITY AND SEDIMENT FLUXES

More detailed analysis was done by studying the velocities and sediment fluxes measured at various cross-shore locations. Near-bed wave-averaged velocity profiles, measured at two locations by the HR-ACVP systems, are shown in Figure 5. The cross-shore positions are indicated by the green vertical bars in Figure 4.

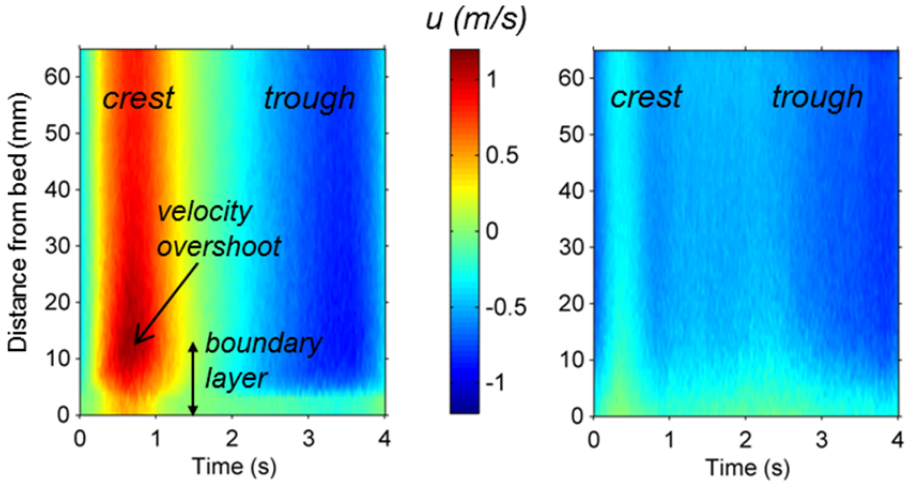

Figure 5: Wave-averaged results of HR-ACVP velocities, RB1 case. Left: fixed frame at location 1 in Figure 4 (pre-breaking, run 3). Right: mobile frame at location 2 in Figure 4 (post-breaking, run 20).

The plots in Figure 5 show well-known features such as the velocity overshoot, which can be used to define the thickness of the wave bottom boundary layer. At location 1, near-bed velocities during the wave crest phase exceed 1 m/s causing bedload sediment transport in the sheet-flow regime (Figure 5 left). During the wave trough phase, velocities are somewhat lower. Due to wave energy dissipation as a result of wave breaking, the orbital velocity amplitude is reduced strongly at location 2 and the time-dependent flow is offshore directed during the complete wave cycle because of the presence of a strong undertow (Figure 5 right). The appearance of bedforms in the surf zone can now also be well explained, since velocities are not high enough to generate sheet-flow sediment transport.

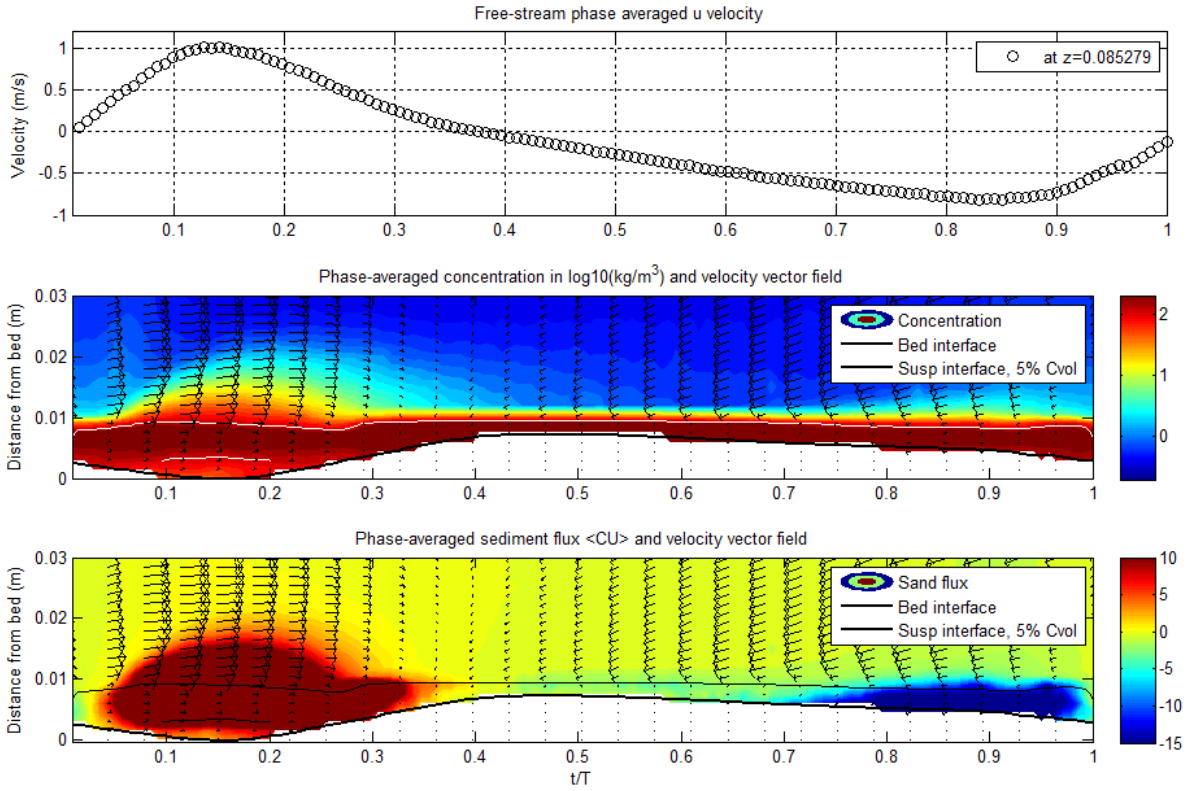

Figure 6: Phase-averaged results of HR-ACVP measurements. Run 6, at x=51 m (pre-breaking). Upper plot: free-stream velocity at z=0.085 m from bed; middle plot: concentrations and velocity vector field; lower plot: sediment fluxes and velocity vector field. The time on the horizontal axis is normalized by the wave period *T* of 4.0 s.

The HR-ACVP can also be used to study sediment concentrations, which in combination with the simultaneously measured velocities, result directly in the near-bed sediment fluxes. Figure 6 shows the phase-averaged concentrations and fluxes in the shoaling zone (x=52 m). During the crest phase, we indeed see transport similar to known sheet-flow layer behavior. The bed-level decreases as sediment is being picked up and returns to its original state near flow reversal. Although the data still have to be validated further, these preliminary results indicate that the HR-ACVP is able to penetrate quite far into the sheet-flow layer. It also becomes evident that the majority of the sediment transport occurs in the thin sheet-flow layer (<2 cm thickness), which is in line with previous research for oscillatory flows (e.g. Ribberink and Al-Salem, 1995; Schretlen, 2012). The trough phase shows similar behaviour, although the thickness of the sheet flow layer is much smaller as a result of the lower velocities under the wave trough. The transport during the crest phase, in the thicker sheet-flow layer, exceeds the transport in the trough phase. Hence, net transport at this location is onshore, which agrees with our observations from Figure 4.

4. OUTLOOK

Upcoming analyses of the data presented herein will include calculations of sediment transport fluxes using the HR-ACVPs together with the CCM+ tanks (near-bed) and the combination of ABS/ADVs (higher in vertical). Our aim is to distinguish the various sediment transport components (current, wave, turbulent), and study how these are affected by wave breaking (RB cases) and shape of the wave group (INB cases). Turbulence estimations using the HR-ACVP and Vectrino Profiler will help us to understand the sediment transport processes we observe.
Moreover, additional experiments in the CIEM wave flume are scheduled as part of the joint UK/Dutch collaboration project SINBAD. A first series will involve additional medium-sand runs, with the aim to study the effects of wave breaking on cross-shore flow non-uniformities and sediment transport rates for one breaking-wave condition in more detail. Subsequently, we will examine hydrodynamics and boundary-layer flow in more detail by a series of rigid-bed experiments, which allows the use of optic measuring instrumentation (PIV, LDA).
The results of the experiments will be used to improve practical sand transport models (e.g. van Rijn, 2007; van der A *et al.*, 2013) that are used in morphodynamic models.

ACKNOWLEDGEMENT

We greatly acknowledge the technical staff of the UPC CIEMLAB for their support throughout the experiments. This work has been supported by European Community's Seventh Framework Programme through the grant to the budget of the Integrating Activity HYDRALAB IV within the Transnational Access Activities, Contract no. 261520, with additional funding from the Dutch Technology Foundation STW and the UK's Engineering and Physical Sciences Research Council (EPSRC) through the SINBAD project.

REFERENCES

Baldock, T.E., Manoonvoravong, P. and Pham, K.S. 2010. Sediment transport and beach morphodynamics induced by free long waves, bound long waves and wave groups. *Coastal Engineering 57(10): 898-916*. doi: 10.1016/j.coastaleng.2010.05.006.

Boers, M. 2005. Surf zone turbulence. *PhD Thesis*, TU Delft, The Netherlands.

Hurther, D., Thorne, P.D., Bricault, M., Lemmin, U. and Barnoud, J.M. 2011. A multi-frequency Acoustic Concentration and Velocity Profiler (ACVP) for boundary layer measurements of fine-scale flow and sediment transport processes. *Coastal Engineering 58(7): 594-605*. doi: DOI 10.1016/j.coastaleng.2011.01.006.

Maddux, T. B., Cowen, E.A. Haller, M.C. and Stanton, T.P. 2006. The Cross-shore sediment transport experiment (CROSSTEX). *Proceedings of the 30th Int.Conf. on Coastal Engineering*. San Diego, USA: 2547-2558

Malarkey, J. and Davies, A.G. 2012. Free-stream velocity descriptions under waves with skewness and asymmetry. *Coastal Engineering 68: 78-95*. doi: 10.1016/j.coastaleng.2012.04.009.

O'Hara Murray, R.B., Hodgson, D.M. and Thorne, P.D. 2012. Wave groups and sediment resuspension processes over evolving sandy bedforms. *Continental Shelf Research 46: 16-30.* doi: DOI 10.1016/j.csr.2012.02.011.

Ribberink, J.S. and Al-Salem, A.A. 1995. Sheet Flow and Suspension of Sand in Oscillatory Boundary-Layers. *Coastal Engineering 25(3-4): 205-225*. doi: 10.1016/0378-3839(95)00003-T.

Roelvink, J.A. and Reniers, A. 1995. LIP 11D Delta Flume Experiments - Data report. *W. D. Hydraulics.* Delft, The Netherlands: 124 pp.

Schretlen, J.L.M. 2012. Sand transport under full-scale progressive surface waves. *PhD Thesis*, University of Twente, The Netherlands.

van der A, D. A., Ribberink, J.S., van der Werf, J.J., O'Donoghue, T., Buijsrogge, R.H. and Kranenburg, W.M. 2013. Practical sand transport formula for non-breaking waves and currents. *Coastal Engineering 76: 26-42.* doi: 10.1016/j.coastaleng.2013.01.007.

van der Zanden, J., Alsina, J.M., Cáceres, I., Buijsrogge, R.H. and Ribberink, J.S. 2013. New CCM technique for sheet-flow measurements and its first application in swash-zone experiments. *Short Course/Conference on Applied Coastal Research,* Lisbon, Portugal, 10 pp.

van Rijn, L.C. 2007. Unified view of sediment transport by currents and waves. I: Initiation of motion, bed roughness, and bed-load transport. *Journal of Hydraulic Engineering-Asce 133(6): 649-667.* doi: 10.1061/(Asce)0733-9429(2007)133:6(649).